ELSEVIER

Nuclear Instruments and Methods in Physics Research A 400 (1997) 185–194

NUCLEAR INSTRUMENTS & METHODS IN PHYSICS RESEARCH Section A

# A three dimensional beam profile monitor based on residual and trace gas ionization

D. Shapira*, T.A. Lewis, J.L. Mosher[1]

*Oak Ridge National Laboratory, Oak Ridge, TN 37831, USA*

Received 8 July 1997; received in revised form 15 August 1997

**Abstract**

A three dimensional beam profile monitor based on tracking the ionization of the residual gas molecules in the evacuated beam pipe is described. Tracking in position and time of the ions and electrons produced in the ionization enables simultaneous position sampling in three dimensions. Special features which make it possible to sample very low beam currents were employed. The characteristics of this detector make it particularly suitable for sampling beams produced at radioactive beam facilities, provided an auxiliary gas feed can be utilized.

## 1. Introduction

Nonintrusive beam sampling was first needed at storage rings and other facilities where high-quality low-emittance charged particle beams had to be stored for extended periods. The first devices which utilize residual gas ionization for beam sampling have been developed and applied extensively at such facilities [1–7]. The notion of nondestructive sampling of beams proved attractive enough to be applied also to extracted beams [8–10]. In all the cases cited above the beam profiles were sampled only along one direction transverse to the beam. Two separate devices had to be used in order to sample two orthogonal projections transverse to the beams' direction of propagation. First attempts to provide two dimensional sampling of the beams' transverse profile appear in [11, 12] but are applicable only when sampling is applied along a very short section along the beam path. More recently [13], true three dimensional sampling was achieved with methods similar to the one described here but which are most suitable for storage rings where a strong transverse magnetic field is also present. All the devices described so far have a low sampling rate and were limited to sampling stored beams or very intense extracted beams, mainly due to background signals and noise in the system. The lowest beam currents which provided relatively clean beam profile samplings were reported in Ref. [9] for beam intensities near 1 pnA. With the emerging interest in radioactive beams, nonintrusive sampling is an attractive option. The construction, instrumentation and testing of a three dimensional beam profile sampler which can operate with very low beam intensities is described in this article.

* Corresponding author. Tel.: +1 423 576 2648; fax: +1 423 574 1268; e-mail: shapira@mail.phy.ornl.gov.

[1] Participant in the Oak Ridge Science and Engineering Semester from Bryn Mawr College, Bryn Mawr, PA.


*PII* S0168-9002(97)01054-1

## 2. Principles of operation

The principle, illustrated in Fig. 1, is based on sweeping out the electrons and the positive ions produced in ionizing collisions between the beam particles and the residual gas molecules in the evacuated beam pipe. The beam particles have large kinetic energies and continue unabated but the residual ions drift in the direction of the electric field (toward the more negative electrode) and the knocked out electrons move in the opposite direction. The extraction electrodes are made with a 94% transmission grid. The charged ions and electrons pass through the grid and are then further accelerated and amplified with Microchannel detectors.

The positive ions produced in the interactions with the "stationary" gas molecule have, on average, very small velocity in the plane transverse to the electric field direction. This is precisely why they are used, as in all previous applications of this method, to infer the original position where the interaction with the beam particle has occurred. By maintaining parallel field lines along which the ions are restricted to move one can project from the position of their arrival back to the interaction region. Spatial resolution is limited in principle by transverse momentum transfer to the residual gas ion by the beam. The lateral displacement is given by

$$\Delta x = \sqrt{\frac{2Mz}{q\Delta V/D}}\, v_\perp = \sqrt{\frac{2Mc^2 z}{q\Delta V/D}}\, \beta_\perp, \qquad (1)$$

where $M$ = mass of residual gas ion, $v_\perp$ = transverse velocity of residual gas ion, $z$ = initial displacement from cathode, $\Delta V$ = applied voltage across detector and $D$ = distance between plates. Typical position resolution achievable with $H_2^+$ ions is around 300 μm (see Ref. [5]).

In our version of this device we also detect the electrons formed in the same interaction. Because of their larger initial velocities the electrons provide somewhat inferior position resolution but they move much faster toward the electrode and their time of arrival is used to trigger a measurement of the drift time of the ions arriving to the opposite electrode. The difference in drift time for ions and electrons generated at the interaction point is given by

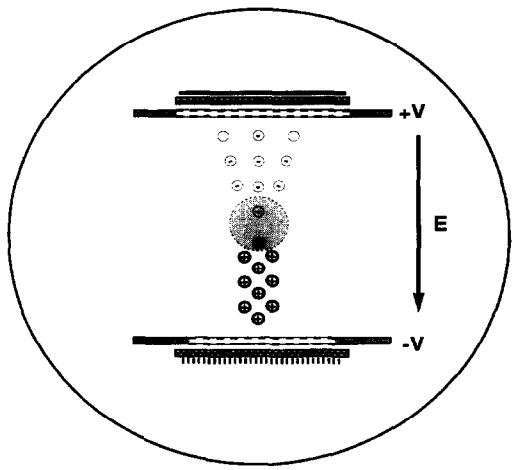


Fig. 1. Principles of detector. Residual gas ion and electron pairs formed in interactions with beam particles are swept vertically in the direction of an applied electric field. Microchannel electron multipliers amplify the signals and provide timing and position signals for the positive ion hits and timing only for electron hits.

$$T = \sqrt{\frac{2MDz}{q\Delta V}} - \sqrt{\frac{2mD(D-z)}{e\Delta V}}. \qquad (2)$$

The variables in use here are the same as in Eq. (1) with the additional variable $m$ = the electron mass. Typical electron drift times are around 1 ns whereas the ion drift times are hundreds of nanoseconds long. The difference in drift times depends on the mass of the ion and the position at which the ion-electron pair was generated.

The anticipated sampling rate can be estimated using calculated energy loss due to gas ionization by the particle passing the sensitive region of the detector. The energy loss is then divided by the energy required to produce an electron ion pair from a gas molecule. The result is a small number, interpreted as an ionization probability that is proportional to the sampling probability (Microchannel efficiency may also be a factor). The numbers in Table 1 were calculated for 6 MeV α particles assuming residual gas pressure of $5 \times 10^{-6}$ torr and a sampling region of 4 cm. In the present situation the interaction probability is low and multiple interactions are very improbable, therefore the ion's charge state will always be the incident particle's charge state. In Table 1, $\Delta$(eV) is the

Table 1
Probability of ion-pair creation predictions for ionization by 6 MeV α particles in the residual gas

| Gas | $T$ (ng/cm$^2$) | $\Delta$ (eV) | Ion pot. (eV) | e+I Prod (eV) | No. of pairs |
|---|---|---|---|---|---|
| $CO_2$ | 56.8 | $42 \times 10^{-3}$ | 15.0 | 200 | $2.1 \times 10^{-4}$ |
| $N_2$ | 36.2 | $26 \times 10^{-3}$ | 15.0 | 196 | $1.4 \times 10^{-4}$ |
| $H_2$ | 2.58 | $6.65 \times 10^{-3}$ | 15.0 | 65 | $1.0 \times 10^{-4}$ |

energy loss calculated for an areal thickness represented by $T$(ng/cm$^2$). The ionization potentials for all these molecules are very similar, but the energy spectrum of electrons emitted following the interaction depends on the process, e.g. impact parameter. The average energy imparted to the ion and electron following an ionizing interaction is nonzero and depends also on the size, charge and mass of the molecule. These numbers are presented in the fifth column Table 1 and are taken from Ref. [15, 16].

In a later section we discuss how one can optimize detector design to obtain good position information rather then doing residual mass spectroscopy! In the following section we describe how a detector based on these principles was built and tested.

## 3. Some construction details and detector tests

The detector construction can be seen in the front and side views shown in Figs. 2 and 3. The electrodes are suspended from one plate using ceramic insulators and all electrical connections are fed through this plate. The sensitive volume is surrounded by two gridded electrodes which allow for 94% transmission of electrons and ions accelerated toward them. On both sides of the volume separating these electrodes we have placed insulating plates lined with field grading strips. The dimensions of the detector assembly are shown for reference (approximately 5" ×5" × 2.5"). Note the the region spanned by the projection of the Microchannel detectors is about half that size resulting in a sensitive volume of 2" × 2" × 2.5".

Signal amplification was achieved with dual, 40 mm diameter, Microchannel plates assemblies [14]. The Microchannel detector's anode plate was substituted by a circuit board with 40 conducting strips (1 mm pitch, 0.6 mm wide) connected to delay line taps providing 2 ns delay per tap. The electrons exiting the Microchannel detector assembly ($10^7$ amplification) hit the anode strips. The signals are read from both sides of the delay line and the delay is decoded into position information. The prompt signal signifying the arrival of the ions was extracted by capacitive coupling to the one of the electrodes used to bias the Microchannel detectors. In this way we were able to obtain both the time and the position of the positive ions' arrival.

There was little doubt that this device would produce adequate position resolution along one transverse direction for which position information was derived from localizing ion hits as they reach the cathode plane. We were more interested in this device's ability to differentiate the ionizing event position in the "vertical" direction, i.e. at what distance between the two detector plates did the event occur. The test setup is shown in Fig. 4. An array of four solid state silicon detectors (SSD#1...SSD#4) was positioned to intercept α particles from a collimated source situated on the opposite side of the beam profile monitor. With this arrangement we could test the ability of the detector to differentiate vertical and horizontal position of particles crossing it as well as study its efficiency as a function of ambient pressure. We could also study the efficiency of this detector by triggering with hits registered in the solid state detectors and then counting the number of ions that reach the MCP detector. The ratio of these numbers yields the probability of ionization by the traversing alpha particles. By triggering on individual detectors we subdivide the detection volume into four distinct regions. By examining the position signal generated in coincidence with hits in individual detectors we can gauge how well the trajectories can be defined. The signal processing scheme used in this test is shown in Fig. 5. The ORPHAS data acquisition system was used for data acquisition and analysis.

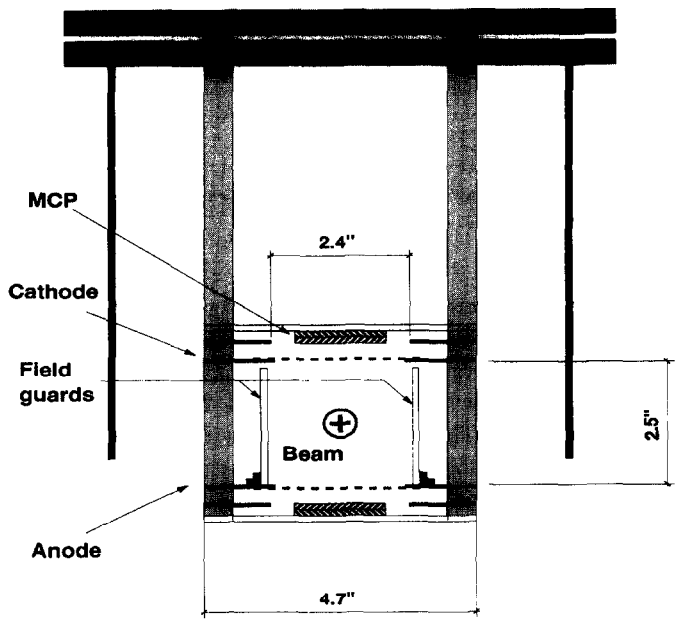


Fig. 2. Front view of detector.

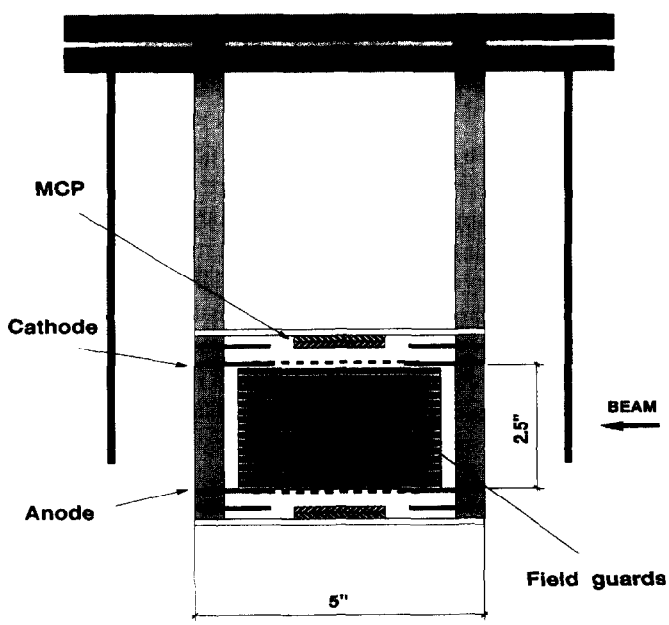


Fig. 3. Side view of detector.

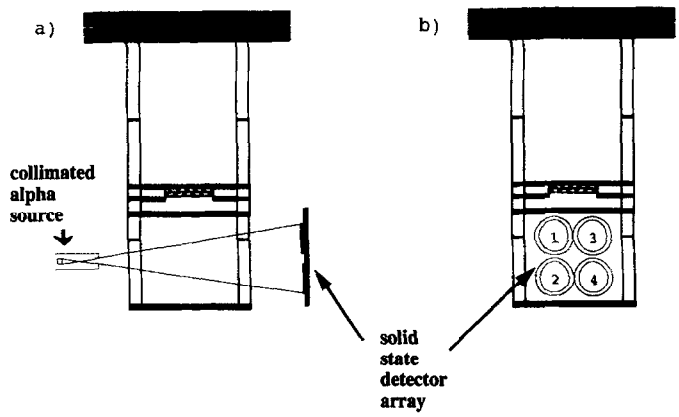


Fig. 4. Setup for efficiency and position sensing tests.

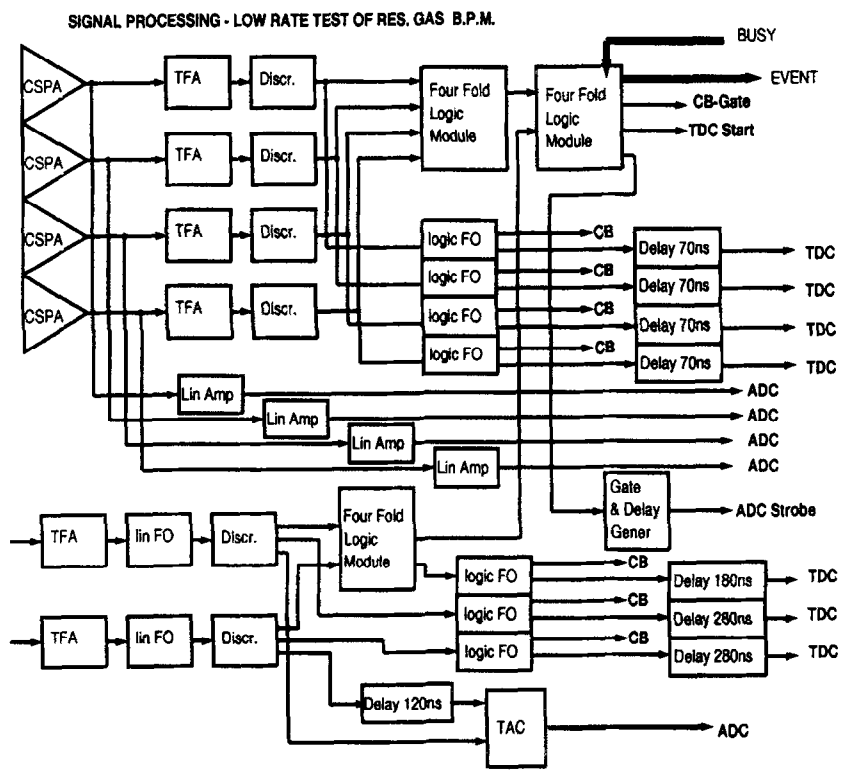


Fig. 5. Signal processing for test of residual gas BPM with alpha particles. Coincidences between solid state detectors and hits on the Microchannel Plate detector were studied.

When we first attempted these tests we found that our spectra contained mostly random counts. Even without the presence of the radiation source, the Microchannel detectors fired at high enough rates to produce the observed rate of random coincidences. We were able to suppress these counts by maintaining all our potential gradients using negatively charged electrodes. In this way electrons generated anywhere outside the desired interaction region are no more attracted to the sensitive region of the detector. Because any particles hitting the material surrounding the sensitive volume produce a large number of secondary electrons that could ionize the gas inside the sensitive volume and generate intolerable background the $\alpha$ particle source was tightly collimated allowing for yields of 30 particles per second. Even with all the precautions some background is expected, e.g. cosmic ray particles hitting the material surrounding the sensitive volume and this background can account for some of the "grass" seen in the following spectra.

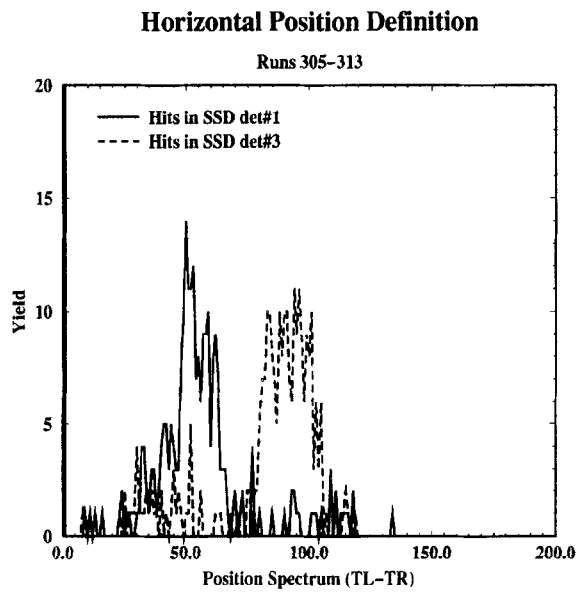


Fig. 6. Position spectra (TL-TR signals from T.A.C) registered in coincidence with two solid state detectors (SSD) positioned about 1.25 in apart in the horizontal direction.

### 3.1. Position resolution

Horizontal position was obtained by recording the time difference between the signals arriving at both ends of the delay line connected to the anode strips. Fig. 6 shows position signals in coincidence with the solid state detectors positioned horizontally apart. Data were taken with ambient pressure of $4 \times 10^{-7}$ torr and about 33 $\alpha$ particles/s hitting the four solid state detectors, and represent some 72 h of counting. In spite of the background present horizontal separation appears to work well.

Vertical position signals were obtained here by recording the ion drift time as registered with a start signal from the solid state detector and the time of signal arrival to both ends of the delay line at the MCP anode strips (TL+TR). As noted in the previous section the drift time depends on vertical position and mass of the ion. In order to better understand and calibrate the spectrum two separate runs were taken. In both cases the system was first evacuated to $5 \times 10^{-7}$ torr and then a controlled leak was introduced bringing the pressure up to $8 \times 10^{-6}$ torr. In one case $N_2$ gas was introduced, and the spectrum shows three prominent peaks corresponding to $N_2^+$, $N^+$ and $N^{++}$. In the other case water vapor was introduced and the spectrum shows two prominent peaks attributed to $H^+$ and $H_2O^+$. The spectra of vertical drift times gated by one of the solid state detectors are shown in Fig. 7. Although some "random" background still persist the data is clustered into discrete groups corresponding to the different ion species that got ionized and accelerated to the MCP for detection. The ion velocity dependence on $\sqrt{m}$ ($m$ = ion mass) is shown in the calibration curve of Fig. 8.

The question is now whether with all the different mass groups arriving at different time intervals one can still get some useful position information out of the ion drift time. One can see from Fig. 9 that we can create a controlled environment (with the $N_2$ gas leak) were we can have vertical position definition. This figure shows a superposition of the drift time spectra taken in coincidence with the two solid state detectors situated one above the other. It shows the shifts in drift time due to spread in vertical position as well as the difference in ion masses. These spectra were taken with residual gas pressure of $8 \times 10^{-6}$ torr (a factor of 20 higher then the ambient pressure during measurements shown in Fig. 6). It is obvious that the mass groups associated with nitrogen are more prominent in these spectra and that they are isolated enough to provide good position information. As expected use

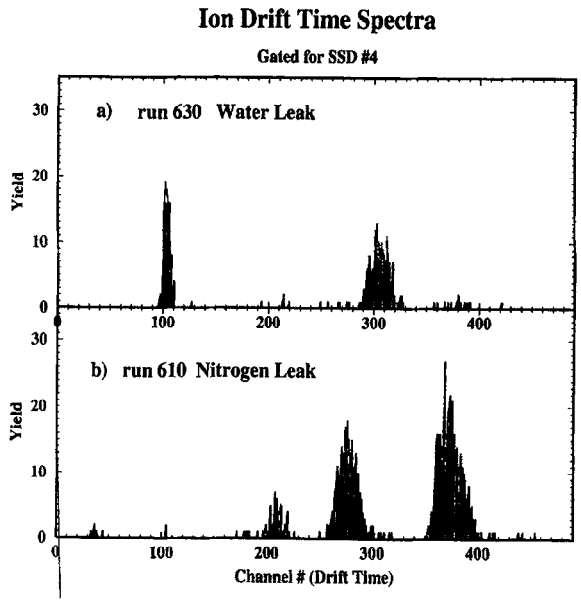


Fig. 7. Spectra with solid state detector no. 4 trigger. Same parameters except that in (a) a $H_2O$ leak and in (b) a $N_2$ leak were introduced.

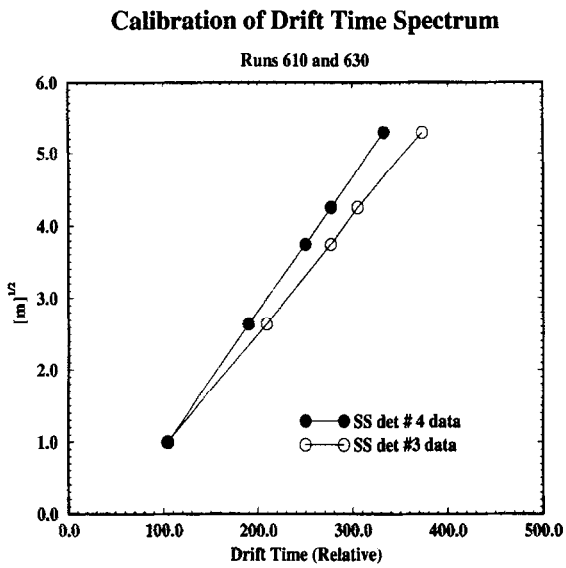


Fig. 8. A calibration curve showing drift time vs. the square root of the mass of the accelerated ion. The ions identified were H, N(doubly charged), N(singly charged), $H_2O$ and $N_2$.

of this method for gleaning position information will depend on the mass spectrum of ions in the residual gas, but we show that can be easily controlled.

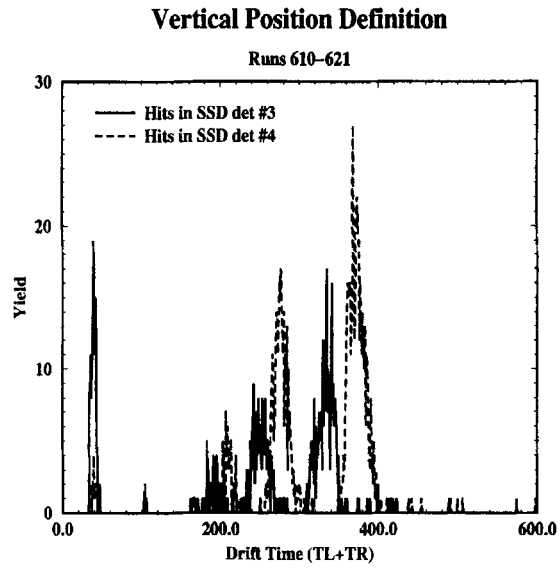


Fig. 9. Drift times recorded in the experiment in coincidence with two solid state detectors (SSD) positioned 1.25 in apart in the vertical direction.

### 3.2. *Detection (ionization) efficiency*

Given the fact that there is always some background which cannot be eliminated, the sampling efficiency of the device is a predictor of its sensitivity at low beam intensities. The calculations which were presented in Table 1 can serve as a guide and the data presented in Table 2 show that the predicted efficiencies come close to reality. The measurements presented in Table 2 were done at three different pressures and demonstrate that the sampling rate is proportional to the ambient pressure. This proportionality is displayed over three orders of magnitude in the double logarithmic plot shown in Fig. 10 which displays measured sampling efficiency as a function of ambient pressure.

## 4. Detector performance

The beam profile monitor has been tested with stable beams and used in conjunction with a Coulomb excitation experiment done with $^{69}As$ beams at the HRIBF facility. Fig. 11 shows the horizontal position signal obtained with 4 ppA (about $10^7$ p/s) $^{48}Ti$

Table 2
Ion detection probability – results from measurement obtained with three residual gas pressure settings

| Gas press.(Torr) | SSD No. 1 | SSD No. 2 | SSD No. 3 | SSD No. 4 |
|---|---|---|---|---|
| $(4.5\pm0.5)10^{-8}$ | $(1.2\pm0.3)10^{-5}$ | $(1.6\pm0.4)10^{-5}$ | $(0.6\pm0.3)10^{-5}$ | $(1.9\pm0.7)10^{-5}$ |
| $(4.5\pm0.5)10^{-7}$ | $(0.8\pm0.1)10^{-4}$ | $(1.7\pm0.1)10^{-4}$ | $(1.2\pm0.2)10^{-4}$ | $(1.7\pm0.2)10^{-4}$ |
| $(5.0\pm0.5)10^{-6}$ | $(1.1\pm0.0)10^{-3}$ | $(2.0\pm0.0)10^{-3}$ | $(1.1\pm0.1)10^{-3}$ | $(1.6\pm0.1)10^{-3}$ |

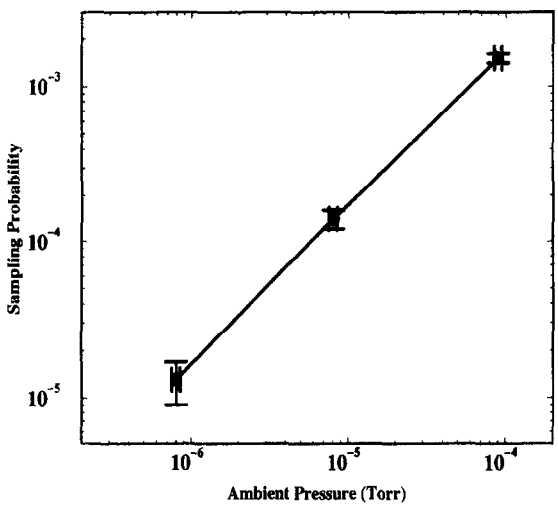


Fig. 10. Sampling rates as a function of ambient pressure.

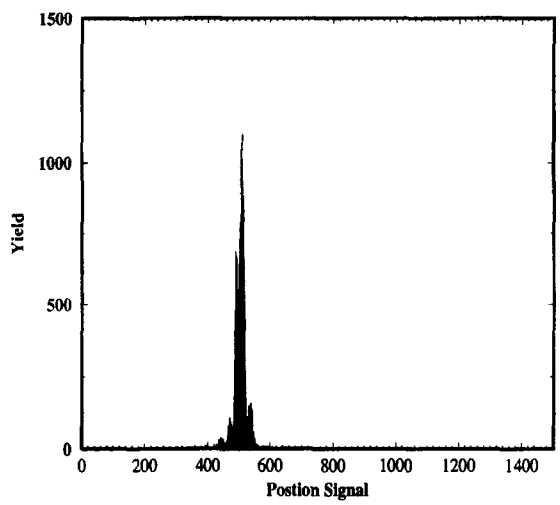


Fig. 11. Horizontal projection of beam spot obtained with 4 particle pA of 160i MeV $^{48}$Ti beam.

beam. The structure seen in the peak shape reflects discontinuities associated with the small size of the beam (less then 2 mm FWHM) and the discrete distribution of charge pickup strips (1mm pitch). In cases where the beam is more diffuse this structure is less pronounced. Note the paucity of background in this spectrum.

Fig. 12 show a two dimensional plot of the beam profile obtained with $^{69}$As beam at intensities near $10^5$ particles per second. We used a nitrogen leak and ran with ambient pressure near $4\times10^{-5}$ torr maintained throughout the experiment. The data shown was accumulated in less then one minute. The $Y$ position was derived from the $N_2$ drift time, and a biased TAC was used to amplify the region around that peak. As can be seen from the two orthogonal projections of the beam profile in Fig. 13, the resolutions in $X$ and $Y$ are comparable and the beam spot in this experiment was about 2–3 mm in diameter.

## 5. Conclusion and further design considerations

The horizontal position resolution attained in our tests can be easily improved on. By using more strips with a smaller pitch one can achieve the expected resolving power of 0.3 mm realized in Ref. [5]. We plan to use this device with extracted beam and may opt to use two dimensional position sensing, such as the resistive layer used in Ref. [4], since the trajectories may diverge and the projection along parallel pick up strips may not provide a true profile. Resolving vertical position by means of drift time is possible as shown in Fig. 6 but will depend on the mass of the ion analyzed and/or the field gradients and detector configuration.

In a simple approach assuming parallel plate geometry we have calculated the time dispersion for a 2 cm beam spot size passing through the middle of the extraction capacitor (8 cm gap). In addition to

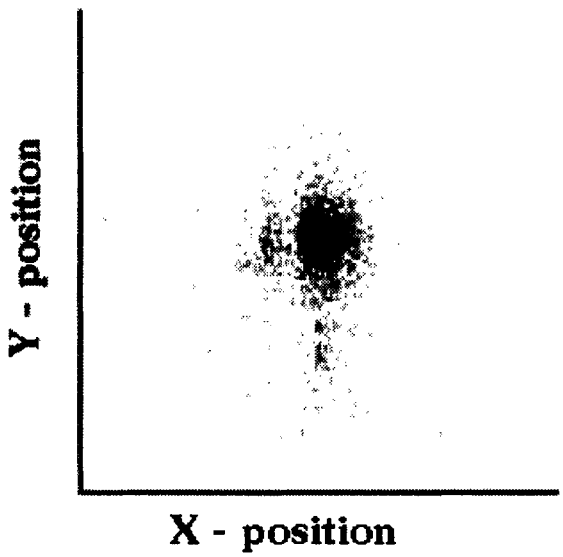


Fig. 12. Two-dimensional beam profile obtained with a beam of $10^5$ $^{69}$As ions per second.

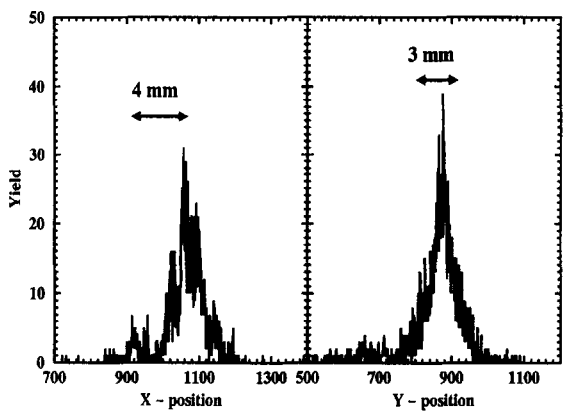


Fig. 13. Horizontal and vertical projection of beam spot obtained with a beam of $10^5$ $^{69}$As ions per second.

the extraction voltage (i.e. the voltage between the anode and cathode) we also maintain an additional accelerating voltage between the cathode and the Microchannel detector entrance. This accelerating voltage is important especially for the positive ion side because the Microchannel efficiency for ion detection peaks at ion energies near 10 keV. We made several calculations where we varied the distance over which the ions are allowed to accelerate as well as the accelerating voltage. Drift times were calculated for

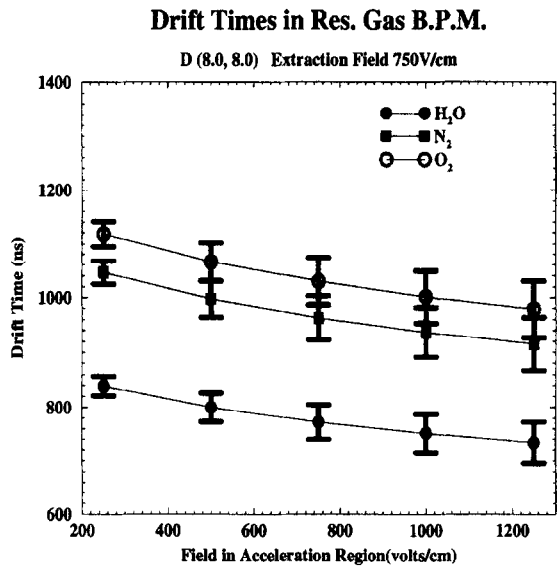


Fig. 14. Drift times from different height as a function of accelerating voltage.

prevailing residual gas molecules: water (mass = 18), $N_2$ (mass = 28) and $O_2$ (mass = 32). Fig. 14 shows the calculated spread in drift time over the 2 cm detection region as a bar straddling the median drift time calculated for $y = 4.0$ cm (the extraction and acceleration regions are both 8 cm deep in the case presented here). For water and $N_2$ there is separation in drift time to allow registering variations over more than 2 cm span of beam spread, but drift time separation for a mixture of $N_2$ and $O_2$ may be too close to separate at some acceleration voltages. When a predominant nitrogen doping is maintained as shown in Fig. 7, we could be sensitive to a large portion of the vertical span of the beam profile monitor. Such methods of doping work very well in our study of extracted beam. In storage rings where very high vacuum must be maintained this may not be necessary since the residual gas at such low pressure is mostly hydrogen.

## Acknowledgements

Oak Ridge National Laboratory is managed by Lockheed Martin Energy Research Corp. for the US Department of Energy under contract number DE-AC05-96OR22464.

## References

[1] T. Hardek, W. Kells, H. Lai, IEEE Trans. Nucl. Sci. NS-28 (1981) 2386.
[2] J. Krider, Nucl. Instr. and Meth. A 278 (1989) 660.
[3] A.N. Stillman, R. Thern, R.L. Witkover, Rev. Sci. Instrum. 63 (6) (1992).
[4] T. Quinteros, R. Schuch, M. Pajek, P. Sigray, H. Cerequist, H. Danared, L. Bagge, A. Filevich, J. Jeansson, A. Kallberg, A. Paal, Nucl. Instr. and Meth. A 333 (1993) 288.
[5] B. Hochadel, F. Albrecht, M. Grieser, D. Habs, D. Schwalm, E. Szmola, A. Wolf, Nucl. Instr. and Meth. A 343 (1994) 401.
[6] W.S. Graves, V. Bharadwaj, D. McGinnis, Nucl. Instr. and Meth. A 364 (1995) 15.
[7] W.S. Graves, Nucl. Instr. and Meth. A 394 (1995) 19.
[8] J.M. Schippers, H.H. Kiewiet, J. Zijlsta, Nucl. Instr. and Meth. A 310 (1991) 540.
[9] R. Anne, Y. Georget, R. Hue, C. Tribouillard, J.L. Vignet, Nucl. Instr. and Meth. A 329 (1993) 21.
[10] M. Bellato, A. Dainelli, S. Marigo, M. Poggi, INFN Annual Report 1995, p. 207.
[11] V.G. Michailov, L.I. Ludin, V.V. Leonov, A.A. Roshchin, V.A. Rezov, V.I. Sklyarenko, A.N. Artem'ev, T. Ya, Rachimbabaev, Proc. European Particle Accelerator Conf., 1994, p. 1743.
[12] V.A. Rezov, L.I. Ludin, V.G. Michailov, V.I. Sklyarenko, A.G. Popeko, A.V. Yeremin, S. Hoffman, V. Ninov, F.P Hesberger, GSI Annual Report, 1996, p. 182.
[13] T. Quinteros, D.R. DeWitt, A. Paal, R. Schuch, Nucl. Instr. and Meth. A 378 (1996) 35.
[14] Dual 40 mm MCP Model 640C, COMSTOCK Inc., 1006 Alvin Weinberg Drive, Oak Ridge, TN 37830, USA.
[15] R. Meinke, W. Nexsen, E. Tsyganov, A. Zinchebko, SSC Report.
[16] F. Sauli, CERN 77-09, 1975.